Deterioration Characteristics and Energy Mechanism of Red-Bed Rocks Subjected to Drying-Wetting Cycles

Kai Huang
Hefei University of Technology School of Resources and Environmental Engineering
Fusheng Zha
Hefei University of Technology School of Resources and Environmental Engineering
Bo Kang (kangbo@hfut.edu.cn)
Hefei University of Technology School of Resources and Environmental Engineering
https://orcid.org/0000-0002-7776-280X
Xianguo Sun
Anhui Huizi Construction Engineering Co.,LTD
Yunfeng Li
China Geological Survey Nanjing Center: Nanjing Geological Survey Center
Jingwen Su
China Geological Survey Nanjing Center: Nanjing Geological Survey Center

Research Article

Keywords: Deterioration characteristics, Energy mechanism, Drying-wetting cycle, Mechanical properties, Microstructural characteristics

Posted Date: June 2nd, 2021

DOI: https://doi.org/10.21203/rs.3.rs-527041/v1

Deterioration characteristics and energy mechanism of red-bed rocks subjected to drying-wetting cycles

Kai Huang[1], Fusheng Zha[1], Bo Kang[1*], Xianguo Sun[2], Yunfeng Li[3], Jingwen Su[3]

[1]*School of Resource and Environmental Engineering, Hefei University of Technology, Hefei, 230009, China*

[2]*Anhui Huizi Construction Engineering Co., LTD, Wuhu, 241000, China*

[3]*Nanjing Geological Survey Center, China Geological Survey, Nanjing, 210016, China*

***Corresponding author**

Ph.D., Bo Kang

School of Resource and Environmental Engineering, Hefei University of Technology

No.193, Tunxi Road, Hefei, 230009

P.R. China

Email: kangbo@hfut.edu.cn

Tel: +86 551 62901523

Mobile: +86 18963794495

Fax: +86 55162901524

Abstract:

The red-bed rocks were chosen and studied by using uniaxial compressive experiment and scanning electron microscopy to investigate the effect of drying-wetting (D-W) cycles on the mechanical properties and microstructural characteristics of red-bed rock. Additionally, the energy mechanism of specimens subjected to drying-wetting cycles was also explained. Experimental results showed that, the stress-strain could be divided into four characteristic stages in the compression failure process. After subjecting to cycles of D-W, the stress-strain curve gradually changed from softening to hardening. At the same time, uniaxial compression strength (UCS) and elastic modulus dropped obviously, while Poisson's ratio gradually raised. Microstructural analysis results indicated that the microstructure of the specimen surface was no longer dense and uniform, and the porosity of tested specimens significantly increased with D-W cycles increasing. As the porosity grew, UCS and elastic modulus gradually declined. According to the first law of thermodynamics, the process of rock failure was an event of energy transfer and conversion. As the number of D-W cycles increased, the energy density of specimens all present linear fell. From the perspective of the theory of energy dissipation, the dissipated energy was essential for rock failure, and closely related to the strength of the specimen. With D-W cycles increasing, the specimens were more prone to failure, and the dissipated energy required for failure decreased gradually.

Keywords: Deterioration characteristics; Energy mechanism; Drying-wetting cycle; Mechanical properties; Microstructural characteristics

1 Introduction

It is well know that the complex environment, such as drying-wetting cycle, groundwater erosion and freezing-thawing, are important factors affecting the deterioration of rock, which related to the success or failure of the geotechnical engineering (Ma et al. 2018; Su et al. 2017; Wu et al. 2013; Yang et al. 2012). It is necessary to consider the impact of the complicated and changeable environment on rock mass stability, especially water. The complex water-rock interaction often occurs

between water and rock mass, which would seriously leads to deterioration and damage of rock engineering characteristics (Yang et al. 2018; He et al. 2014). Ma et al. (2018); Liu et al. (2018); and Lu et al. (2017) reported that engineering structures often suffer from complex and varied natural environments, such as frequent rainfall and evaporation, groundwater level changing, and fluctuation of water level in reservoir area. During these processes, the rock would be subjected to the cyclic dry and wet, and accelerate the deterioration process of rocks. Thus, the drying-wetting cycle is one of the most common and influential water-rock interaction.

In recent years, the influence of drying-wetting cycles on the physical and mechanical properties of rock has been studied by many researches (Liu et al. 2018; Zhou et al. 2017; Torres-Suarez et al. 2014; Hoven et al. 2003; Gökceoğlu et al. 2000). By running drying-wetting cycle tests on rock samples, the evolution of physical properties including bulk density, weight loss, porosity and P-wave velocity were studied. The results showed that the bulk density, weight loss, and P-wave velocity decreased, whereas the porosity raised with the increase of the number of drying-wetting cycles (Pardini et al. 1996; Özbek, 2014). Khanlari et al. (2015) and Hale et al. (2003) reported that the uniaxial compressive strength of sandstone was reduced insignificantly with the number of drying-wetting cycles increasing, which indicated the limited influences of cyclic drying-wetting to samples. However, Huang et al. (2018) and Yang et al. (2018) concluded that the mechanical properties of sandstone deteriorated significantly under the wetting-drying cycles. Similar work performed by Wang et al. (2020) and Deng et al. (2019) also indicated that the irreversible progressive damage to the rock caused by the cyclic drying-wetting. Besides, Hua et al. (2016, 2017) proposed that the failure characteristics of sandstone changed from brittle to ductile at higher wetting-drying cycles.

Furthermore, the drying-wetting cycles not only induced the deterioration of the physical and mechanical properties of rock, but also caused irreversible damage to the microstructure of rocks. With the development of testing techniques, the scanning electron microscope, computed tomography scanning, and nuclear magnetic resonance, has been gradually used to study the microscopic evolution of rocks under drying-

wetting cycles (He et al. 2020; Ma et al. 2020; Chen et al. 2018; Devarapalli et al. 2017). By using scanning electron microscope, Zhang et al. (2014), Liu et al. (2018) and Yang et al. (2019) investigated the effect of different drying-wetting cycles on the microstructure of rock samples, the results showed that the cohesion of rock particles was gradually weakened, and the porosity increased significantly after repeated water absorption and loss. Chen et al. (2019, 2018) analyzed the damage of drying-wetting cycle to rock strength and microstructure systematically. By conducting a series of experiments, Yao et al. (2020) found that the root of deformation and failure of rock was the failure of the microstructure, and the weakening of rock mechanical properties was an external expression of the microstructure.

As mentioned above, most researches mainly focused on qualitative analysis or quantitative characterization from mechanical tests and microscopic tests including calcareous rock (Cardell et al. 2003), sandstone (Wedekind and Ruedrich, 2006), and dolostone (Benavente et al. 2007). However, limited studies have paid attention to the energy damage mechanisms of rock. Rock energy dissipation is an essential property of rock deformation and failure, which mainly reflects the generation, sustainable development, weakening and ultimate loss of micro-defects inside the rock. The energy dissipation of rock can reflect the internal structural damage in the rock. Additionally, the researches of red-bed rocks has mostly focused on the disintegration characteristics of soft rocks (Kurlenya and Oparin 1996; Doostmohammadi et al. 2009; Qian et al. 2009). However, the research on the slightly weathered rock of red-bed is rare.

Given the above, focusing on the slightly weathered rock of red-bed taken from the Tongcheng, Anhui Province, China, the strength deterioration and micro-structure changes of red-bed rock under drying-wetting cycles were studied in this paper. Uniaxial compression tests and Scanning Electron Microscope (SEM) were carried out on specimens exposed to deionized water drying-wetting cycles. Meanwhile, after subjected to drying-wetting cycles, energy damage mechanisms were analyzed from the perspective of energy dissipation.

2 Materials and Methods

2.1 Materials and Specimen preparation

The rock materials used in this study were the slightly weathered rock of red-bed collected from the city of Tongcheng city Anhui province, China. Some essential physical parameters were measured: water content (4.03%), density (2.33 g/cm^3), porosity (12.50%) and specific gravity (2.77). In addition, the chemical composition of the tested specimens was analyzed by X-ray fluorescence (XRF), and shown in Table 1. The XRD results of the tested rock are shown in Fig. 1, in which a large amount of quartz and mica have been identified.

According to the standard testing method recommended by the International Society for Rock Mechanics and Rock Engineering, 24 tested specimens were cut into cylinders with the size of Φ 50×100 mm (diameter × height), the difference of the height was less than 0.5 mm and the surface evenness was less than 0.1 mm(ISRM, 1981; Brown, 1981; Zhou et al. 2012).

2.2 Test methods

2.2.1 Drying-wetting procedure

According to the methods suggested by Khanlari et al. (2015), D-W cycles test was performed in the laboratory to study its effect on the mechanical properties and microstructure of rock. Considering the operability of drying-wetting cycles experiment and the actual situation, every drying-wetting cycle was divided into two parts, drying (from saturated to dry state) and wetting (from dry to saturated state). In each cycle, specimens were submerged into deionized water for 24h to reach the saturated state, and then they were taken out and dried in an oven at 110℃ for 24 hours. In this study, 0 (representing the natural state), 1, 3, 5, 7, and 10 D-W cycles were designed for various specimens.

2.2.2 Uniaxial compressive strength test

The UCS was determined based on the methods suggested by ISRM (1981), the purpose of the uniaxial compression experiment is to determine the uniaxial compressive strength, elastic modulus, and other parameters of rock. This experiment

was carried out on ZTCR-2000 rock triaxial testing machine, which can automatically collect the data of load and the axial radial deformation during the experiment until the rock was broken. Based on the collected data, the rock stress-strain curve, and the uniaxial compressive strength of the specimens can be obtained.

2.2.3 Microstructural analysis

After being subjected to their designated numbers of D-W cycles, specimens were cut into small pieces with an approximate size of 5 mm × 5 mm × 5 mm, and the surface of tested specimens was cleaned using a hairbrush. Then, immersed in liquid nitrogen and freeze-dried in the Alpha 1-4 LDplus Freeze Dryer for 24 h. In order to improve the electrical conductivity, the specimens were vacuum metalized before the examination. Finally, morphology observation was carried out using a JSM-6490LV scanning electron microscope (SEM).

All the experiments were performed at an ambient temperature of 25±0.1℃.

3 Results and discussion

3.1 Stress-strain characteristics

In order to investigate the effect of D-W cycles on the deformation properties of red-bed rock, the stress-strain curves of specimens subjected to various D-W cycles are plotted in Fig. 2.

Generally, the axial stress-axial strain curve presented four distinct stages, including initial compaction stage, linear elastic deformation stage, pre-peak failure stage and post-peak softening stage. (a) Initial compaction stage (OA): under an external force, due to the closing of the micro-cracks inside the red-bed rock, the specimens were gradually compacted, and the axial stress-axial strain curve showed a concave shape. (b): Linear elastic deformation stage (AB): After the internal micro-cracks were closed and compacted, the axial stress- strain curve showed a nearly linear relationship in this stage. (c) Pre-peak failure stage (BC): The curve showed an apparent concave shape, the micro-cracks developed and gathered until specimens reached the peak strength and ultimately failed. (d) Post-peak softening stage (CD): After reaching

the peak strength, the stress decreased with the strain rapidly increasing, and a failure surface was formed with the development of the micro-cracks.

Moreover, as shown in Fig. 2, the specimen that did not experience cycles of D-W demonstrated the highest failure stress, whereas the corresponding failure strain was the minimum. When the strength reaches the maximum value, the strength drops sharply, and the failure mode was typical brittle failure. As the number of D-W cycles raised, the peak strength decreased, while the corresponding strain increased significantly, the stress-strain curves gradually showed more apparent strain-hardening. Which indicated that with the increase of the number of D-W cycles, more micro-cracks were generated, and accelerate the damage imparted to the rock.

It also can be seen from Fig. 2 that the stress-stain curves of all cases were approximately linear in the elastic deformation stage, whose slopes significantly fell as the number of D-W cycles extended. This indicating that specimens were deformed more after exposure to D-W cycles. And the shear failure of specimens subjected to D-W cycles could take place at a more considerable strain than that of specimens without D-W cycles.

3.2 Evolution of mechanical properties

According to the uniaxial compression stress-strain curve, the peak strength of the tested specimens subjected to different D-W cycles could be obtained via the equation (1), the elastic modulus and Poisson's ratio can be obtained via the equations (2) and (3).

$$\sigma = \frac{P}{A} \tag{1}$$

$$E = \frac{\sigma}{\varepsilon_y} \tag{2}$$

$$\mu = \frac{\varepsilon_x}{\varepsilon_y} \tag{3}$$

In these equations, where σ is the axial stress (MPa), P is the maximum load (kN), A is the cross-sectional area of the specimen (mm^2), E is the Elastic modulus (MPa), ε_y is the axial strain (10^{-2}), μ—Poisson's ratio, and ε_x is the lateral strain (10^{-2}).

Fig. 3 showed the variations of the uniaxial compression strength (UCS) of the

tested specimens after experiencing different D-W cycles. The results indicated that strength was slackened significantly as the number of D-W cycles increased, from 18.94 MPa in the initial state to 8.07 MPa after 10 D-W cycles. A high strength reduction rate appeared in the early stage of D-W, which become relative slower in the later stage. After experiencing 10 cycles of D-W, the reduction percentage of UCS from the original (unexposed to D-W) specimens increased to 57.34%. It also could be proved that an exponential equation could describe the relationship between UCS and number of drying-wetting cycles. The best-fit line is plotted in Fig. 3, and the best fitting equation can be obtained as follows:

$$UCS(n)=UCS_0-3.99\ln(1+n)=18.94-3.99\ln(1+n),\ R_1^2=0.925 \quad (4)$$

In addition, the damage of a material such as red-bed rock due to D-W cycles can be represented by the changed of degradation degree D_d, which indicates the change in the strength of the material. The D_d has been widely used to express the change of rock mechanical parameters due to cyclic drying-wetting conditions, freezing-thawing conditions, and thermal treatment (Talukdar et al. 2018; Chen et al. 2019). D_d was calculated here using the following formula:

$$D_{dUCS}=\left(1-\frac{UCS_n}{USC_0}\right)\times 100\% \quad (5)$$

Where D_{dUCS} is the total degradation degree of UCS of specimens subjected to n drying-wetting cycles, UCS_n is the uniaxial compressive strength of specimens subjected to n drying-wetting cycles, and UCS_0 is the initial uniaxial compressive strength of specimens.

The results of D_{dUCS} was shown in Fig. 3. It can be seen that, UCS decreased with the increase of the D-W cycles. The corresponding degradation degrees of the UCS for n = 1, 3, 5, 7, and 10 were 16.58%, 21.53%, 30.95%, 46.55%, and 57.35%, respectively. The UCS degenerated significantly in the initial stage, whereas with further increases the number of D-W cycles, the UCS degenerated more gradually. It could be concluded that significant relationship existed between the uniaxial compression strength of the red-bed rock and the number of D-W cycles.

Based on the equation (2), the results of elastic modulus of specimens after subjecting to D-W cycles are presented in Fig. 4.

Fig. 4 showed that with D-W cycles increasing, the elastic modulus (E) decreased while Poisson's ratio gradually raised. In Fig. 4(a), when the number of cycles increased from 0 to 10, the elastic modulus reduced from 3.26 to 1.27 GPa by 60.85%. In Fig. 4(b), the maximal Poisson's ratio of the red-bed rock was 29.42%, which increased rapidly in the first five D-W cycles. The Poisson's ratio extended to 28.62% after experiencing 5 D-W cycles, then the increasing trend slowed down, and converged to its maximum after undergoing the tenth D-W cycles.

In addition, the relationship between elastic modulus, Poisson's ratio and the number of D-W cycles could be described by an equation, as showed in equations (6) and (7). The R^2 of the linear function were greater than 0.969 (see Fig. 4), indicating that the obtained function fits well with the experimental data. In order to further analyze the softening effect of D-W cycling on specimens, the degradation degree of the elastic modulus was obtained using the equation (8). As shown in Fig. 4(a), the degradation degree of elastic modulus was 11.37%, 23.14%, 38.34%, 50.89%, and 60.85%, respectively, corresponding to n 1, 3, 5, 7, and 10. The degradation degree curves of E showed a rapidly rising trend, then slowly developed, as n grew from 1 to 10.

$$E(n)=E_0-0.75\ln(1+n)=3.26-0075\ln(1+n),\ R_3^2=0.969 \quad (6)$$

$$\mu(n)=0.29-0.08e^{-0.47n},\ R_5^2=0.980 \quad (7)$$

$$D_{dE}=\left(1-\frac{E_n}{E_0}\right)\times 100\% \quad (8)$$

Where D_{dE} is the total degradation degree of elastic modulus, E_n is the elastic modulus of specimens subjected to n D-W cycles, and E_0 is the initial elastic modulus of specimens.

3.3 Effects of D-W cycles on the microstructure characteristics

The Scanning Electron Microscopy (SEM) at 1000 times magnification was used to monitor the evolution of microstructure of specimens after experiencing 1, 3, 5, 7

and 10th cycles of D-W. The results are illustrated in Fig. 5.

It can be seen from Fig. 5 (a) that the surface of the specimen in the initial state is relatively smooth, the structure is complete and dense, with few surface microcracks. However, after experiencing 1 D-W cycle, the hydraulic intrusion caused micro-crack propagation and the surface of the tested specimen became rough, as shown in Fig. 5 (b). With the increase of cycles, the microstructure of the rock specimen surface was no longer dense, and the particle shape gradually evolved from massive and flat to disordered. After the third D-W cycle, the number of micro-pores gradually increased. Additionally, loose particles appeared on the surface with pores unevenly distributed, as shown in Fig. 5 (c). After undergoing the fifth D-W cycle, the effect of cycles on the internal erosion of the specimen progressively deepened and micro-pores on the surface continued to develop, and the flaky aggregations were appeared on the surface, as shown in Fig. 5 (d). After undergoing the seventh D-W cycle, some clay mineral began to be dissolved, and the flaky aggregations decreased, as shown in Fig. 5 (e). Finally, as shown in Fig. 5 (f), when the number of D-W cycles reached up to 10, the original small pores gradually penetrated and merged into a large one under the water-rock interaction.

These results indicated that the D-W cycles weakened the connectivity of the internal structure of the specimen to a certain extent, and aggravated the initiation and development of fractures. Compared to the initial state, the microstructure of the specimen, and the size, shape, distribution of pore on the specimen surface significantly changed. After subjected to D-W cycles, the microstructure of the rock specimen surface was no longer dense and uniform, the clay particles evidently lost, and the flaky aggregations were appeared within the surface. As the number of D-W cycles increased, the continuously dissolution of the flaky aggregations filled within the rock mass structures, and formed a new structural plane. Furthermore, the pores expanded and secondary pores developed. Finally, the small pores gradually penetrated and merged into large pores, which may have led to abrupt instability in the rock's strength.

In order to further study the microstructure evolution of red-bed after D-W cycles,

image analysis software was used to qualitatively analyze the SEM analysis results. For this purpose, Image-Pro Plus (IPP) software was choose and could be used to obtain the porosity of the red-bed after subjected the D-W cycles [34,48]. Based on the results of SEM images by IPP image analysis software, the percentage curve of cumulative porosity with the increase of the number of cycles, and the graphical representation of these functions was shown is plotted in Fig. 6. It was evident that the porosity gradually increased with the number of D-W cycles increasing. In order to describe porosity evolutions, a function was employed to fit the experimental data and the best fitting equation was obtained as follows:

$$P(n)=25.11-12.64e^{0.14n},\ R_6^2=0.992 \quad (9)$$

The fitting result of porosity evolutions is illustrated in Fig. 6. As the D-W cycle number increased, the porosity of specimen gradually grew. The porosity of the red-bed rock extended to 18.88% after undergoing the third D-W cycles. Since then, the increment trend accelerated, and finally slowly increased, to its maximum of 21.72% at tenth D-W cycles. It can be concluded that, when the number and width of pore cracks progressively increased, some micro-pores were gradually penetrated or merged into the larger pores, and new micro-fractures were generated under the action of D-W cycles.

3.4 Relationship between mechanical and microstructure characteristics

Additionally, Salvoni et al. (2016) and Saksala et al. (2016) suggested that the damage to the microstructure of the rock was the fundamental reason for the weakening of the rock's mechanical properties. Therefore, the evolutionary relationship between microstructure and mechanical properties should also be critical factors. The evolutionary relationships between the uniaxial compressive strength, elastic modulus and porosity of the rock are shown in Fig. 7.

Results in Fig. 7 showed that, these two evolutionary relationships were all linear. As the porosity gradually increased, the uniaxial compressive strength and elastic modulus gradually fell, which indicated that the evolution of the mechanical properties

was closely related to the change in microstructure. In order to describe the evolutionary relationship between the porosity and the uniaxial compressive strength and elastic modulus, a function was employed to fit the experimental data and the best fitting equation was obtained as follows:

$$UCS(n)=31.90-1.06n,\ R_7^2=0.946 \quad (10)$$

$$E(n)=5.90-0.21n,\ R_8^2=0.980 \quad (11)$$

According to the above analysis, the degradation of mechanical properties was caused by damage to the rock internal structure. During the process of D-W cycles, the water weakened the interaction between mineral particles and induced the change in internal pore size, porosity, and other microstructural characteristics. The porosity raised with the increased number of cycle, and the internal structure of rock was damaged, resulting in the degradation of mechanical properties.

4 Rock Energy Evolution of D-W cycles

4.1 Energy composition of the rock

It is known from the first law of thermodynamics that the process of rock failure is essentially an event of energy transfer and conversion, and the evolution of energy is the internal cause of macroscopic deformation. Based on the energy theory of rock proposed by Xie et al. (2009), the procedure of energy conversion of the specimen during uniaxial loading is shown in Fig. 8. As given by Fig. 8(a), the energy of rock under the external load consisted of energy inputting, energy storage and dissipation, and energy releasing. During uniaxial loading, the rock constantly absorbed energy from mechanical energy, i.e., input energy. The input energy was stored in the specimen in the form of elastic energy, and some amount of elastic energy was converted into dissipated energy in the initial compressive stage. During the pre-peak failure stage, the dissipated energy density of the rock gradually increased. When the load reached peak stress, the dissipated energy significantly extended, the elastic energy stored in the specimen was gradually released in the form of kinetic energy and fracture energy, and the specimen began to deform and eventually destroyed (Li et al. 2020; Xiao et al. 2019; Gong et al. 2019). The relationship between elastic energy density (U^e) and dissipated

energy density (U^d) is illustrated in Fig. 8(b).

As mentioned previously, the deformation and failure of the specimen were caused by a combination of energy dissipation and energy release. Energy dissipation could produce irreversible deformation and deteriorate the microstructure and the strength (Xie et al. 2004). Based on the first law of thermodynamics, the inputted energy density could be expressed as:

$$U=U^d+U^e \tag{12}$$

Where U^d is the density of dissipated energy commonly consumed for internal damage and crack propagation, U^e is the released elastic energy density. Moreover, the energy equation during the uniaxial compressive test could be expressed as:

$$U=\int_0^{\varepsilon}\sigma d\varepsilon \tag{13}$$

$$U^e=\frac{1}{2}\sigma\varepsilon^e=\frac{\sigma^2}{2E_e}=\frac{\sigma^2}{2E} \tag{14}$$

$$U^d=U-U^e=\int_0^{\varepsilon}\sigma d\varepsilon-\frac{\sigma^2}{2E} \tag{15}$$

Where σ is the axial stress, ε is the axial strain, and E_e is the unloading elastic modulus. Since there is no unloading process in the uniaxial compression test, the initial elastic modulus E is used instead of E_e (Li et al. 2014; Zhou et al. 2020).

4.2 Energy evolution of red-bed rock under D-W cycles

By analyzing energy evolution in the uniaxial compressive test under the D-W cycles and using the calculation method mentioned in Sect. 4.1, the input energy density, dissipated energy density and elastic energy density of specimens at different cycles could be obtained (see Fig. 9).

As given by Fig. 9, the three energy densities all presented nonlinear growth with the increase of strain. The inputted energy density grew fastest, followed by the elastic energy density and then dissipated energy density. The curve of the elastic energy density was closer to the total inputted energy density, which indicated that a large amount of the external input energy was transformed into the elastic energy. In contrast, few elastic energy was converted into dissipated energy and accumulated in the specimen. Besides, it can be seen from Fig. 9 that the total inputted energy density and

elastic energy density of specimens in the initial state were the highest. With D-W cycles increasing, the energy densities gradually decreased. The result proved that a high compressive strength usually represented a strong energy storage capacity, and the uniaxial compressive strength declined significantly under cyclic D-W. The energy storage capacity of the specimen gradually weakened, and these characteristics were also confirmed by previous observations shown in Fig. 2.

To further describe the relationships between the inputted energy density (u_n), elastic energy density (u_n^e) of specimens and the D-W cycles, a linear function was used to fit the variation laws of energy density at peak strength. The linear relationships between u_n, u_n^e and the number of D-W cycles (n) are shown in Fig. 10. The coefficient correlation R^2 of the fitting functions in Fig. 10 were all greater than 0.923, which mean the linear function could well describe the relationship between u_n, u_n^e and the number of D-W cycles (n). It can be seen from Fig. 10 (a) that as the number of D-W cycles increased, the u_n and u_n^e significantly decreased. In the initial state, the value of u_n and u_n^e were 66.88 KJ/m^3 and 54.28 KJ/m^3, respectively. After experiencing 10 D-W cycles, the value was reduced to 34.60 KJ/m^3 and 24.46 KJ/m^3, which indicated that with the increasing number of D-W cycles, the limit of the specimen energy accumulation declined. The reduction in specimen energy accumulation limit represents when the energy generated by the external load accumulates inside the specimens, it may easily exceed the energy accumulation limit, which accelerates the energy release process. Furthermore, as the number of D-W cycles increased, the dissipated energy density gradually fell (shown in Fig. 10 (b)), which indicated that the D-W cycles accelerated the internal micro-cracks and development and expansion of micro-pores, and the specimens subjected to D-W cycles were more prone to failure. Similar results were also reflected by the microstructure characteristics shown in Fig. 5. In addition, the dissipated energy required for specimen failure gradually decreased.

4.3 Energy mechanism of rock failure

It can be seen from Fig. 9, the dissipated energy density remained unchanged in

the initial compressive stage, and was mainly used for development and expansion of internal fracture. With the increase of strain, the UCS and dissipated energy density gradually increased. Once the stress reached the peak strength, the elastic energy density was rapidly released, the dissipated energy density significantly raised, and then the specimen failed. Furthermore, as given by Fig. 11, with the increase of D-W cycles, the porosity gradually grew, and UCS gradually decreased, accompanied by the decreasing dissipation energy of specimens. This represented that during D-W cycles, specimens continuously absorbed the external energy, resulting in the deterioration of the microstructure and reduction the UCS. As some part of dissipated energy was consumed by fracture propagation and evolution of specimen, the dissipated energy density of the specimen gradually reduced with the increase of D-W cycles.

Fig. 12 showed the evolving relationship between UCS and porosity and dissipated energy. As given by the Fig. 12, as the dissipated energy gradually decreased, the porosity gradually increased, while UCS gradually decreased. The result illustrated that the dissipated energy density was closely related to the damage of specimens, and damage caused by the rock deformation process could be regarded as continuous energy dissipation.

As mentioned above, the energy dissipation is the essential property of rock deformation and destruction, which reflects the process of continuous development of micro-cracks inside the rock and weakening process of strength. When the loading conditions are consistent, the damage evolution of the loading process depends on the initial damage state inside the rock. The energy dissipation ratio of the failure site reflects not only the deformation process of the rock before the failure, but also the failure degree of the rock under different D-W cycles. Therefore, the greater the dissipation energy ratio of destruction, the more serious the initial failure degree of rock was. The relationship between the energy distribution ratio of the rock failure and the D-W cycle is shown in Fig. 13. With the increase of D-W cycle, the dissipation energy ratio increased and the elastic energy ratio declined, which indicated that a larger

number of D-W cycles led to more severe damage inside the rock and a lower energy accumulation efficiency. After that, the UCS of the specimen gradually fell.

5 Conclusions

In this study, a series of tests were performed on the red-bed rock to investigate the deterioration characteristics of the specimen subjected to D-W cycles. Meanwhile, energy evolution characteristic and damage mechanisms of specimens were analyzed. The main conclusions are as follows:

(1) The stress-strain curve of specimens exhibit four distinct stages in the compression failure process, including initial compaction stage, elastic stage, pre-peak failure stage and post-peak softening stage. With the increase of the D-W cycles, the stress-strain curves of specimen gradually changed from softening to hardening.

(2) UCS and elastic modulus decreased obviously with the number of D-W cycles increasing, while the Poisson's ratio gradually increased A relatively higher degradation rate in strength and elastic modulus appeared at the end of the 3rd cycle of D-W.

(3) With the number of cycles increasing, the microstructure of the rock specimen surface was no longer dense and uniform. By IPP image analysis software, we found that the porosity of tested specimen subjected to D-W cycles increased significantly. As the porosity increased, UCS and elastic modulus gradually fell down.

(4) The input energy density and dissipated energy density gradually extended with the increasing strain; the elastic energy density increased first and then declined. As the number of D-W cycles increased, the energy density of specimens all presented a linear downward trend.

(5) From the perspective of the theory of energy dissipation, the dissipated energy is the essential attribute of rock failure, and closely related to the strength of the specimen. With the increasing of D-W cycles, the specimens were more prone to destruction, and the dissipated energy required for specimen failure gradually decreased. After that, the UCS of the specimen gradually fell.

Declaration of competing interest

All authors declare that there are no possible conflicts of interest.

Acknowledgement

This research is financially supported by the National Natural Science Foundation of China (grant No. 41877262, 42030710, and 41672306), the Natural Science Foundation of Anhui Province (1908085QD168) and Geological Survey projects (DD20189250, and DD20190261) of the China Geological Survey.

References

Benavente D, Martínez-Martínez J, Cueto N, García-Del-Cura MA (2007) Salt weathering in dual-porosity building dolostones. Engineering Geology 94(s3-4):215-226. https://doi.org/10.1016/j.enggeo.2007.08.003

Brown ET (1981) Rock characterization testing and monitoring. Pergamon Press.

Cardell C, Rivas T, Mosquera MJ, Birginie JM, Moropoulou A, Prieto B (2003) Patterns of damage in igneous and sedimentary rocks under conditions simulating sea-salt weathering. Earth Surface Processes and Landforms 28 (1), 1-14. https://doi.org/10.1002/esp.408

Chen H, Huang H, Qian C (2018) Study on the deterioration process of cement‐based materials under sulfate attack and drying–wetting cycles. Structural Concrete 19(4): 1225-1234. https://doi.org/10.1002/suco.201700038

Chen XX, He P, Qin Z (2018) Damage to the Microstructure and Strength of Altered Granite under Wet–Dry Cycles. Symmetry 10(12): 716. https://doi.org/10.3390/sym10120716

Chen XX, Gong YP (2019) Features of Shear Strength Parameters Reflecting Damage to Rock Caused by Water Invasion-Loss Cycles. Geotechnical and Geological Engineering, 37, 1919–1929. https://doi.org/10.1007/s10706-018-0733-2

Chen SJ, Jiang TQ, Wang HY, Feng F, Yin D-W, Li XS (2019) Influence of cyclic wetting‐drying on the mechanical strength characteristics of coal samples: A laboratory‐scale study. Energy Science and Engineering 7(6): 3020-3037. https://doi.org/10.1002/ese3.476

Deng HF, Zhang YC, Zhi YY (2019) Sandstone dynamical characteristics influenced by water-rock interaction of bank slope. Advances in Civil Engineering 2019. https://doi.org/10.1155/2019/3279586

497 Devarapalli RS, Islam A, Faisal TF, Sassi M, Jouiad M (2017) Micro-CT and FIB–SEM
498 imaging and pore structure characterization of dolomite rock at multiple scales.
499 Arab J Geosci 10: 361. https://doi.org/10.1007/s12517-017-3120-z
500 Doostmohammadi R, Moosavi M, Mutschler T, Osan C (2009) Influence of cyclic
501 wetting and drying on swelling behavior of mudstone in south west of Iran.
502 Environ Geol 58: 999. https://doi.org/10.1007/s00254-008-1579-3
503 Gökceoğlu C, Ulusay R, Sönmez H (2000) Factors affecting the durability of selected
504 weak and clay-bearing rocks from Turkey, with particular emphasis on the
505 influence of the number of drying and wetting cycles. Engineering Geology 57(3-
506 4):215-237. https://doi.org/10.1016/S0013-7952(00)00031-4
507 Gong FQ, Yan JY, Luo S. Li, XB (2019) Investigation on the Linear Energy Storage
508 and Dissipation Laws of Rock Materials Under Uniaxial Compression. Rock
509 Mechanics and Rock Engineering 52: 4237–4255. https://doi.org/10.1007/s00603-
510 019-01842-4
511 Hale PA, Shakoor A (2003) A laboratory investigation of the effects of cyclic heating
512 and cooling, wetting and drying, and freezing and thawing on the compressive
513 strength of selected sandstones. Environmental and Engineering Geoscience
514 9(2):117-130. https://doi.org/10.2113/9.2.117
515 He MC, Sun XM, Zhao J (2014) Advances in interaction mechanism of water (gas) on
516 clay minerals in China. International Journal of Mining Science and Technology
517 24: 727-735. https://doi.org/10.1016/j.ijmst.2014.10.009
518 He R, Zheng S, Gan VJL, Wang ZD, Fang JH (2020) Damage mechanism and
519 interfacial transition zone characteristics of concrete under sulfate erosion and
520 Dry-Wet cycles. Construction and Building Materials 255: 119340.
521 https://doi.org/10.1016/j.conbuildmat.2020.119340
522 Hua W, Dong S, Li Y, Wang Q (2016) Effect of cyclic wetting and drying on the pure
523 mode II fracture toughness of sandstone. Engineering Fracture Mechanics 153:
524 143–150. https://doi.org/10.1016/j.engfracmech.2015.11.020
525 Hua W, Dong SM, Peng F, Li KY, Wang QY (2017) Experimental investigation on the
526 effect of wetting-drying cycles on mixed mode fracture toughness of sandstone.
527 International Journal of Rock Mechanics and Mining Sciences 93: 242–249.
528 https://doi.org/10.1016/j.ijrmms.2017.01.017
529 Huang SY, Wang JJ, Qiu ZF, Kang K (2018) Effects of cyclic wetting-drying conditions
530 on elastic modulus and compressive strength of sandstone and mudstone.

Processes 6(12): 234. https://doi.org/10.3390/pr6120234

Hoven SJV, Solomon DK, Moline GR (2003) Modeling unsaturated flow and transport in the saprolite of fractured sedimentary rocks: Effects of periodic wetting and drying. Water resources research 39(7):1186. https://doi.org/10.1029/2002WR001926

ISRM (1981) Rock characterization, testing and monitoring. In: Brown ET (ed) ISRM suggested methods. Pergamon, Oxford

Khanlari G, Abdilor Y (2015) Influence of wet–dry, freeze–thaw, and heat–cool cycles on the physical and mechanical properties of Upper Red sandstones in central Iran. Bulletin of engineering geology and the environment 74: 1287–1300. https://doi.org/10.1007/s10064-014-0691-8

Kurlenya MV, Oparin VN (1996) Scale factor of phenomenon of zonal disintegration of rock, and canonical series of atomic and ionic radii. Journal of Mining Science 32(2): 81-90. https://doi.org/10.1007/BF02046676.

Li YR, Huang D, Li XA (2014) Strain rate dependency of coarse crystal marble under uniaxial compression: strength, deformation and strain energy. Rock mechanics and rock engineering 47(4): 1153-1164. https://doi.org/10.1007/ s00603-013-0472-x

Li JL, Hong L, Zhou KP, Xia CH, Zhu LY (2020) Influence of Loading Rate on the Energy Evolution Characteristics of Rocks under Cyclic Loading and Unloading. Energies 13(15): 4003. https://doi.org/10.3390/en13154003

Liu DQ, Wang Z, Zhang XY, Wang Y, Zhang XL (2018) Experimental investigation on the mechanical and acoustic emission characteristics of shale softened by water absorption. Journal of Natural Gas Science and Engineering 50: 301-308. https://doi.org/10.1016/j.jngse.2017.11.020

Liu XR, Jin MH, Li DL, Zhang L (2018) Strength deterioration of a Shaly sandstone under dry–wet cycles: a case study from the Three Gorges Reservoir in China. Bulletin of Engineering Geology and the Environment 77: 1607–1621. https://doi.org/10.1007/s10064-017-1107-3

Lu YL, Wang LG, Sun XK, Wang J (2017) Experimental study of the influence of water and temperature on the mechanical behavior of mudstone and sandstone. Bulletin of Engineering Geology and the Environment 76: 645–660. https://doi.org/10.1007/s10064-016-0851-0

Ma CQ, Wang P, Jiang LS, Wang CS (2018) Deformation and control countermeasure

565 of surrounding rocks for water-dripping road-way below a contiguous seam goaf.
566 Processes 6: 77. https://doi.org/10.3390/pr6070077
567 Ma CQ, Li HZ, Niu Y (2018) Experimental study on damage failure mechanical
568 characteristics and crack evolution of water-bearing surrounding rock.
569 Environmental Earth Sciences 77: 23. https://doi.org/10.1007/s12665-017-7209-1
570 Ma TT, Wei CF, Yao CQ, Yi PP (2020) Microstructural evolution of expansive clay
571 during drying–wetting cycle. Acta Geotechnica 1-12. https://doi.org/10.1007/
572 s11440-020-00938-4
573 Qian QH, Zhou XP, Yang HQ, Zhang YX, Li XH (2009) Zonal disintegration of
574 surrounding rock mass around the diversion tunnels in Jinping II Hydropower
575 Station, Southwestern China. Theoretical and Applied Fracture Mechanics 51:
576 129- 138. https://doi.org/10.1016/j.tafmec.2009.04.006.
577 Özbek A (2014) Investigation of the effects of wetting–drying and freezing–thawing
578 cycles on some physical and mechanical properties of selected ignimbrites. B
579 Bulletin of Engineering Geology and the Environment 73: 595–609. https://
580 doi.org/10.1007/s10064-013-0519-y
581 Pardini G, Guidi G V, Pini R, Regüésb D, Gallartb F (1996) Structure and porosity of
582 smectitic mudrocks as affected by experimental wetting—drying cycles and
583 freezing—thawing cycles. Catena 27(3-4): 149-165. https://doi.org/10.1016/0341-
584 8162(96)00024-0
585 Ramandi HL, Mostaghimi P, Armstrong RT, Saadatfar M, Pinczewski WV (2016)
586 Porosity and permeability characterization of coal: A micro-computed tomography
587 study. International Journal of Coal Geology, 154-155:57-68. https://doi.org/
588 10.1016/j.coal.2015.10.001
589 Salvoni M, Dight PM (2016) Rock damage assessment in a large unstable slope from
590 microseismic monitoring-MMG Century mine (Queensland, Australia) case study.
591 Engineering Geology 210: 45–56. https://doi.org/10.1016/j.enggeo. 2016.06.002
592 Saksala T (2016) Modelling of Dynamic Rock Fracture Process with a Rate-Dependent
593 Combined Continuum Damage-Embedded Discontinuity Model Incorporating
594 Microstructure. Rock Mechanics and Rock Engineering 49: 3947–3962.
595 https://doi.org/10.1007/s00603-016-0994-0
596 Su YH, Fang YB, Li S, Su Y, Li X (2017) A one-dimensional integral approach to
597 calculating the failure probability of geotechnical engineering structures.
598 Computers and Geotechnics. 90: 85–95. https://doi.org/10.1016/j.compgeo.

2017.05.019

Talukdar M, Roy DG, Singh TN (2018) Correlating mode-I fracture toughness and mechanical properties of heat-treated crystalline rocks. Journal of Rock Mechanics and Geotechnical Engineering, 10(1): 91-101. https://doi.org/10.1016/j.jrmge.2017.09.009

Torres-Suarez MC, Alarcon-Guzman A, Moya BD (2014) Effects of loading–unloading and wetting–drying cycles on geomechanical behaviors of mudrocks in the Colombian Andes. Journal of Rock Mechanics and Geotechnical Engineering 6(3): 257-268. https://doi.org/10.1016/j.jrmge.2014.04.004

Wu XZ (2013) Trivariate analysis of soil ranking-correlated characteristics and its application to probabilistic stability assessments in geotechnical engineering problems. Soils and Foundations 53, 540–556. https://doi.org/10.1016/j.sandf.2013.06.006

Wang LQ, Yin Y, Huang BL, Dai ZW (2020) Damage evolution and stability analysis of the Jianchuandong Dangerous Rock Mass in the Three Gorges Reservoir Area. Engineering Geology, 265: 105439. https://doi.org/10.1016/ j.enggeo.2019.105439

Wedekind W, Ruedrich J (2006) Salt-weathering, conservation techniques and strategies to protect the rock cut facades in Petra/Jordan. In: Heritage, Weathering and Conservation. Proceedings of the International Heritage, Weathering and Conservation Conference. Taylor & Francis, London, pp. 261-268.

Xiao FK, Wang HR, Liu G (2019) Study on Multiparameter Precursory Information Identification of the Fracture of Yellow Sandstone. Advances in Civil Engineering. 2019: 7676801. https://doi.org/10.1155/2019/7676801

Xie HP, Peng RD, Ju Y (2004) Energy dissipation of rock deformation and fracture. Chinese Journal of Rock Mechanics and Engineering 23(21):3565–3570. https ://doi.org/10.1016/j.jnucm at.2004.03.002

Xie HP, Li LY, Peng RD, Ju Y (2009) Energy analysis and criteria for structural failure of rocks. Journal of Rock Mechanics and Geotechnical Engineering 1(1):11–20. https://doi.org/10.3724/SP.J.1235.2009.00011

Yao WM, Li CD, Zhan HB, Zhou JQ, Criss RE (2020) Multiscale Study of Physical and Mechanical Properties of Sandstone in Three Gorges Reservoir Region Subjected to Cyclic Wetting–Drying of Yangtze River Water. Rock Mechanics and Rock Engineering 53: 2215–2231. https://doi.org/10.1007/s00603-019-02037-7

633 Yang J, Tao ZG, Li BL, Yang G, Li HF (2012) Stability assessment and feature analysis
634 of slope in Nanfen Open Pit Iron Mine. International Journal of Mining Science
635 and Technology 22: 329–333. https://doi.org/10.1016/j.ijmst.2012.04.008
636 Yang XJ, Wang JM, Zhu C, He MC, Gao Y (2019) Effect of wetting and drying cycles
637 on microstructure of rock based on SEM. Environmental earth sciences 78(6): 183.
638 https://doi.org/10.1007/s12665-019-8191-6
639 Yang XJ, Wang JM, Hou DG, Zhu C, He MC (2018) Effect of dry-wet cycling on the
640 mechanical properties of rocks: a laboratory-scale experimental study. Processes
641 6(10): 199. https://doi.org/10.3390/pr6100199
642 Zhang ZH, Jiang QH, Zhou CB, Liu XT (2014) Strength and failure characteristics of
643 Jurassic Red-Bed sandstone under cyclic wetting–drying conditions. Geophysical
644 Journal International 198(2): 1034-1044. https://doi.org/10.1093/ gji/ggu181
645 Zhou YX, Xia K, Li XB, Li HB, Ma GW, Zhao J (2012) Suggested methods for
646 determining the dynamic strength parameters and mode-i fracture toughness of
647 rock materials. International Journal of Rock Mechanics and Mining Sciences 49
648 (1):105–112. https://doi.org/10.1007/978-3-319-07713-0_3
649 Zhou ZL, Cai X, Chen L, Gao WZ, Zhao Y (2017) Influence of cyclic wetting and
650 drying on physical and dynamic compressive properties of sandstone. Engineering
651 Geology 220: 1-12. https://doi.org/10.1016/j.enggeo.2017.01.017
652 Zhou Y, Sheng Q, Li N, Fu XD (2020) The Influence of Strain Rate on the Energy
653 Characteristics and Damage Evolution of Rock Materials Under Dynamic
654 Uniaxial Compression. Rock Mechanics and Rock Engineering 53: 3823–3834.
655 https://doi.org/10.1007/s00603-020-02128-w
656

List of Figures and Tables

Table 1 Chemical content of tested specimens

Silicon	Calcium	Aluminium	Iron	Potassium	Magnesium	Sodium	other
57.82%	9.26%	16.98%	5.21%	4.47%	3.65%	0.53%	2.38%

Figures

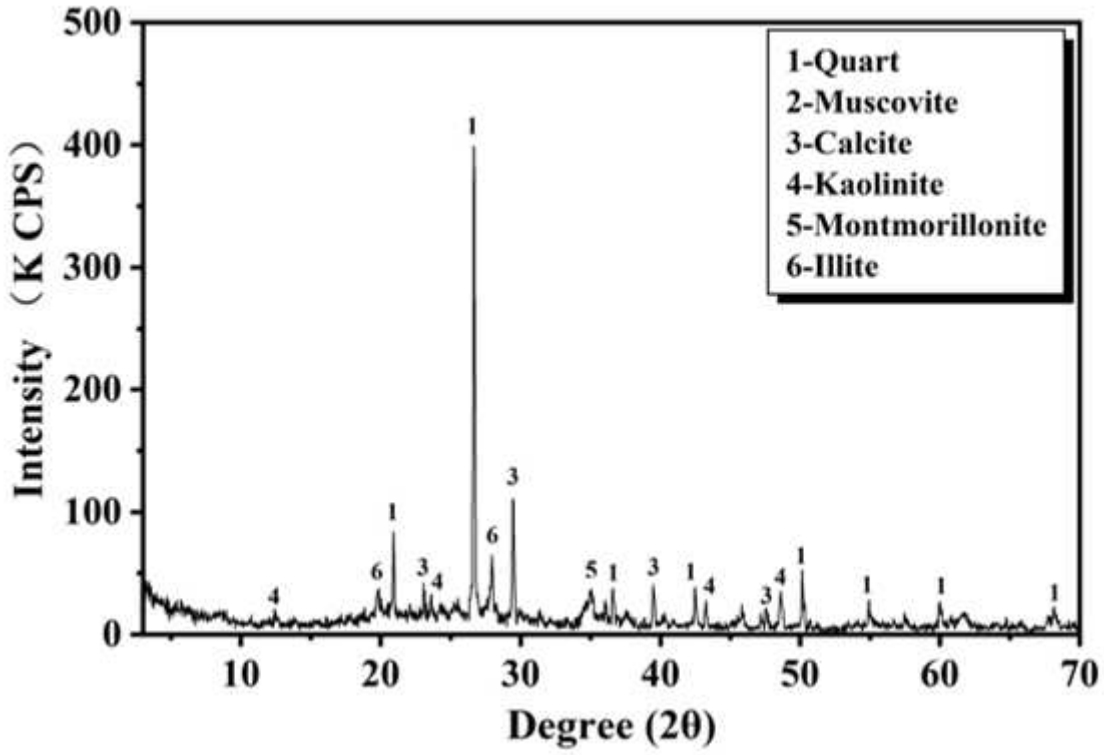

Figure 1

XRD results of tested rock

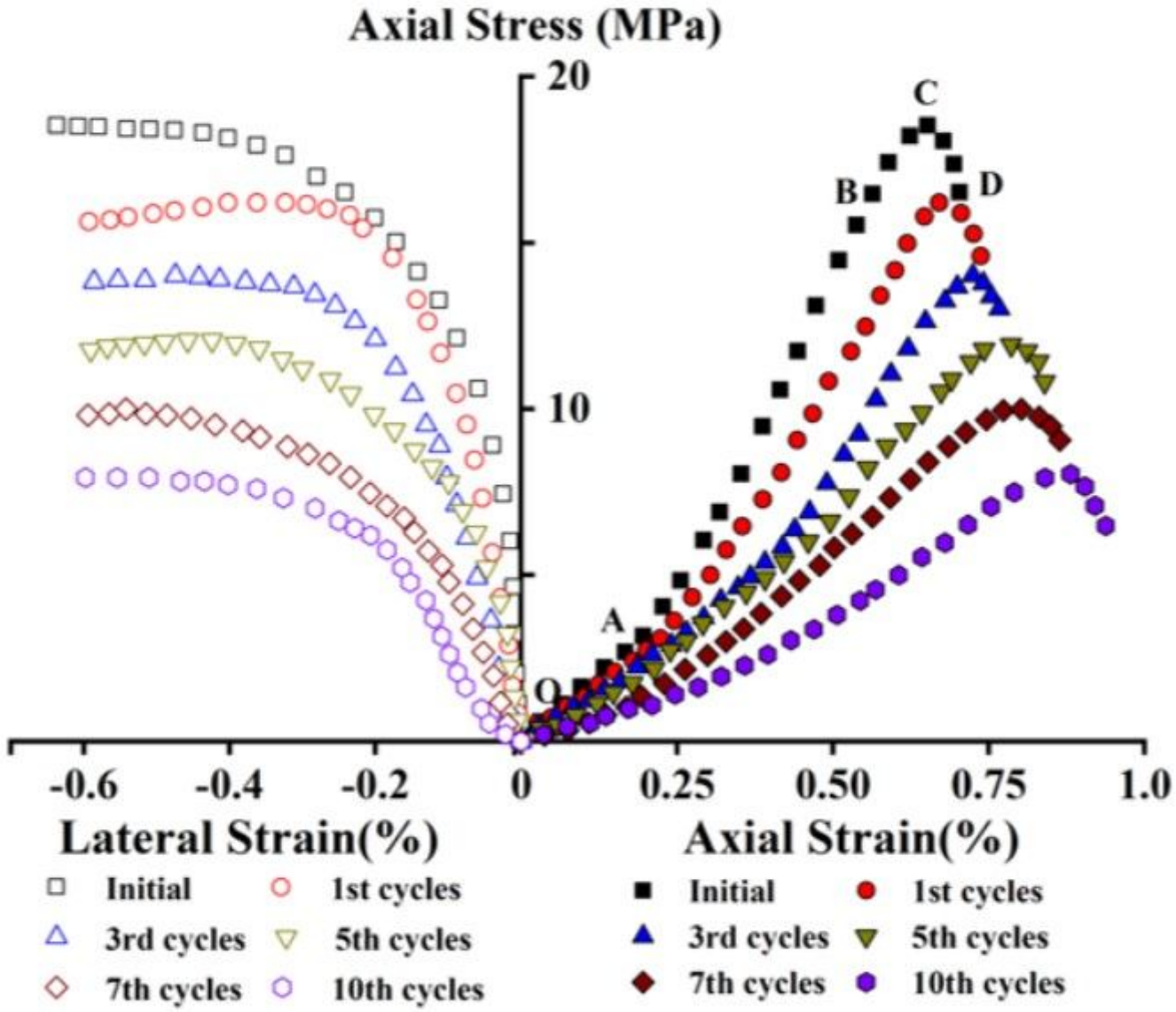

Figure 2

Stress-strain curves of specimens subjected to different drying-wetting cycles

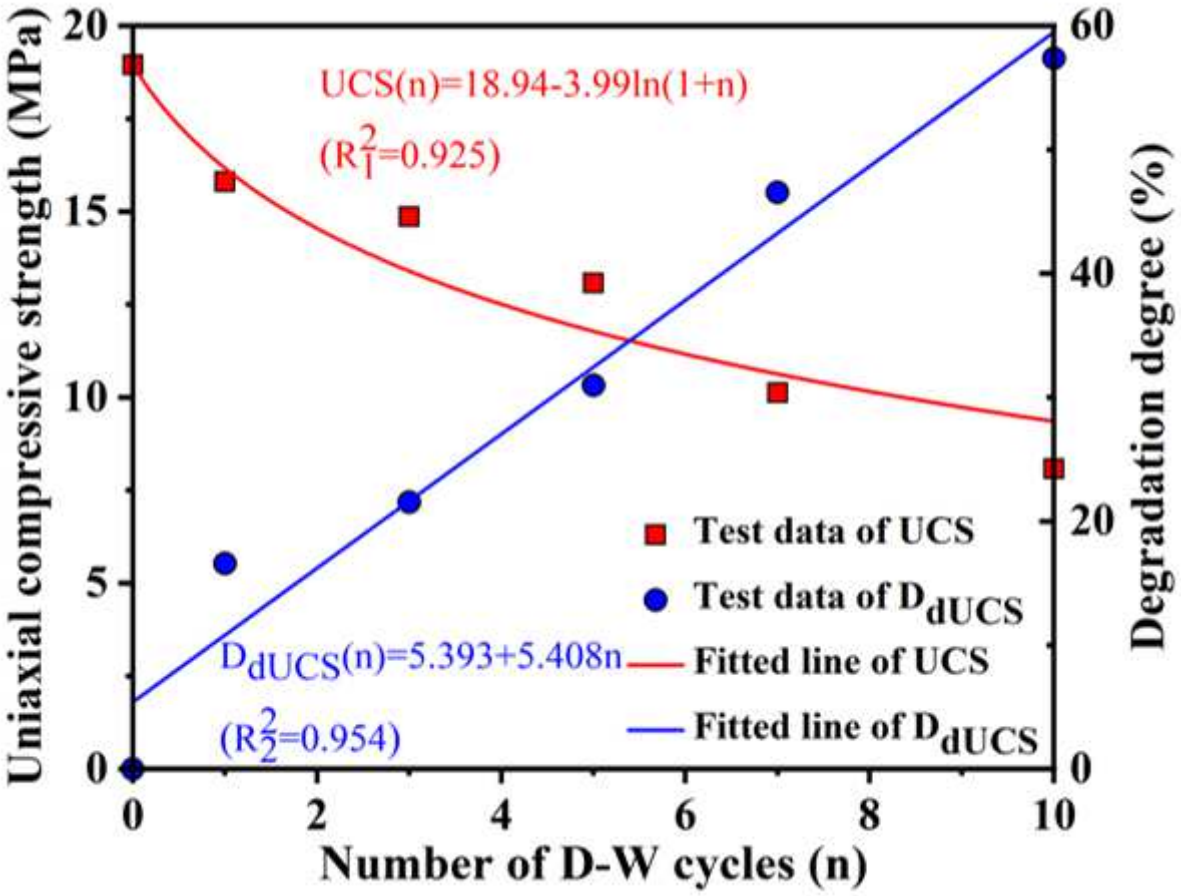

Figure 3

Variation of UCS of specimens after subjecting to D-W cycles

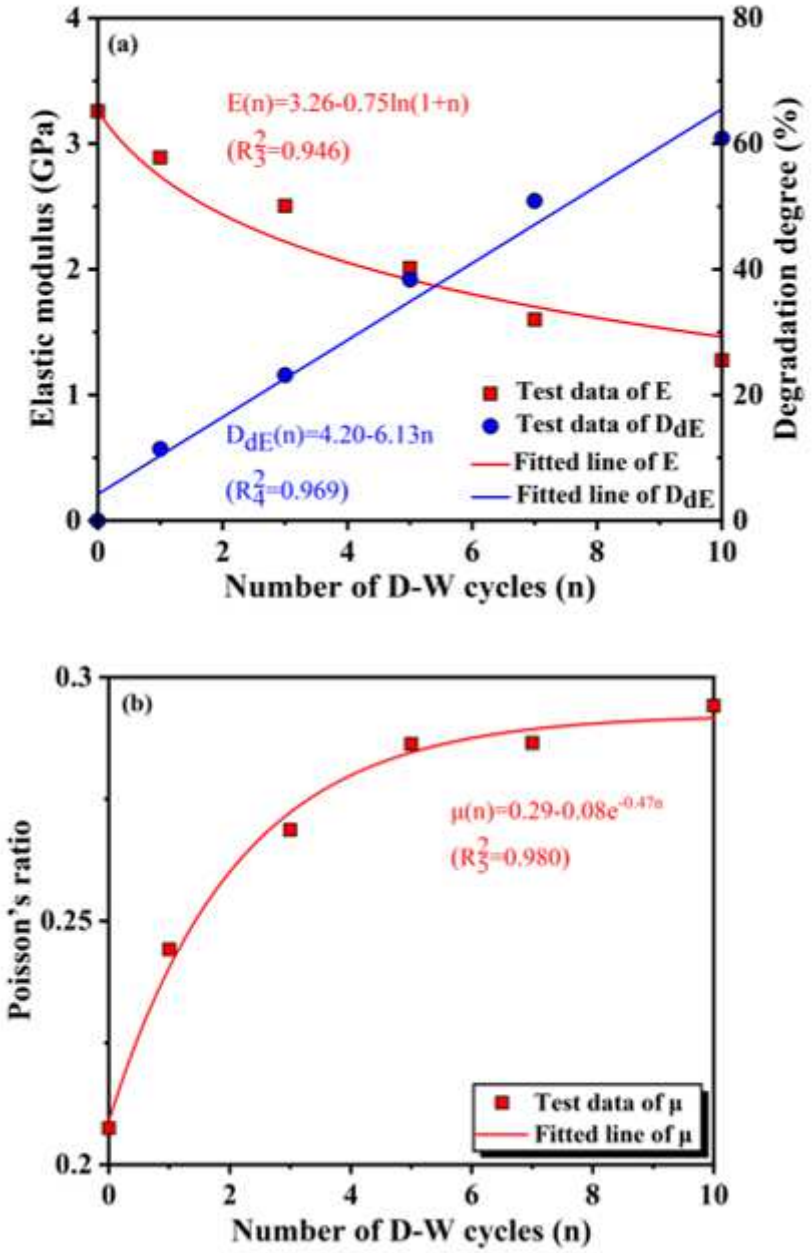

Figure 4

Variation of mechanical parameters of specimens after subjecting to D-W cycles: (a) elastic modulus, (b) Poisson's ratio

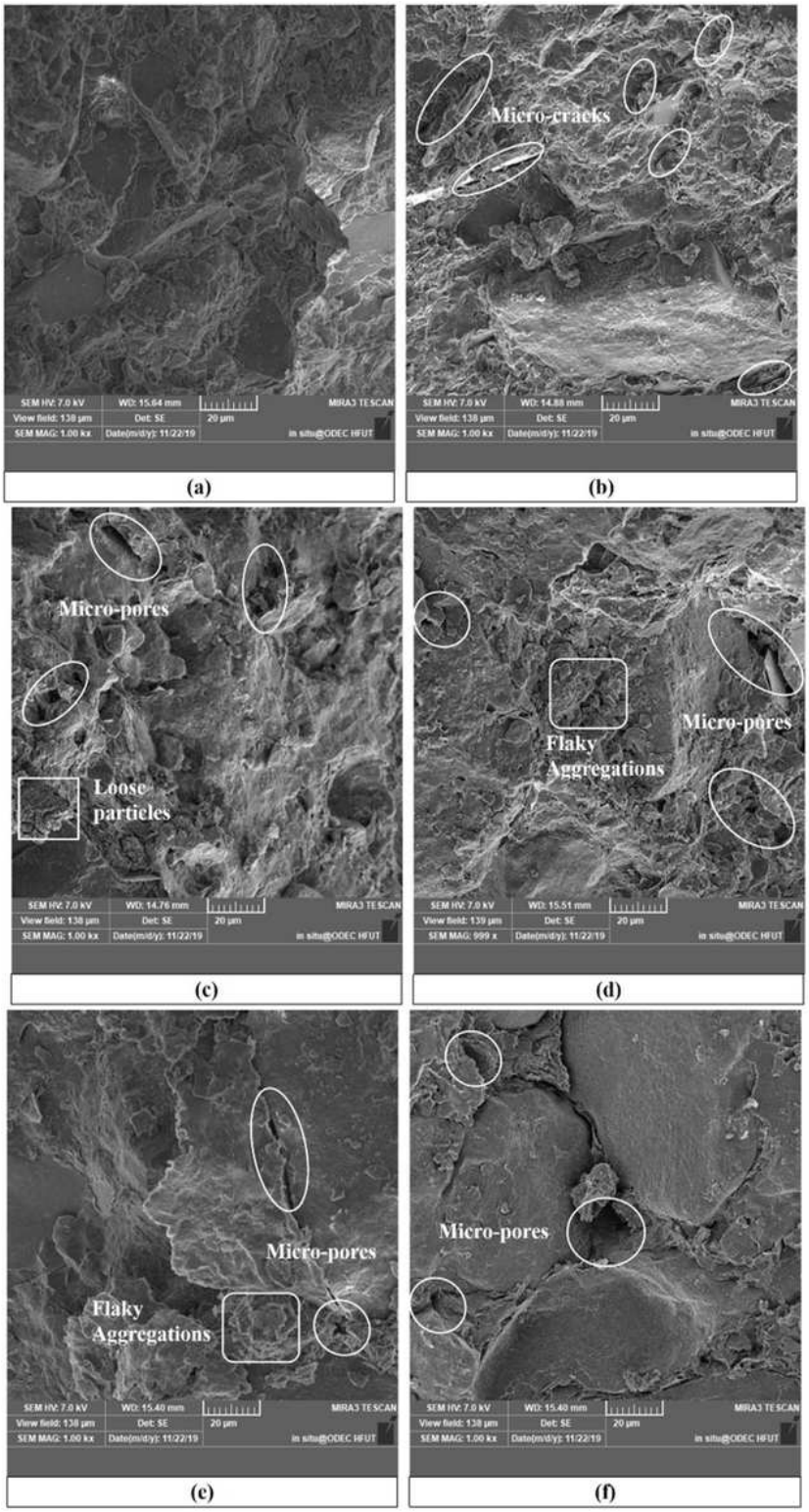

Figure 5

Microstructure characteristics of the tested specimens subjected to: (a) Initial; (b) 1 cycles; (c) 3 cycles; (d) 5 cycles; (e) 7 cycles; (f) 10 cycles of D-W

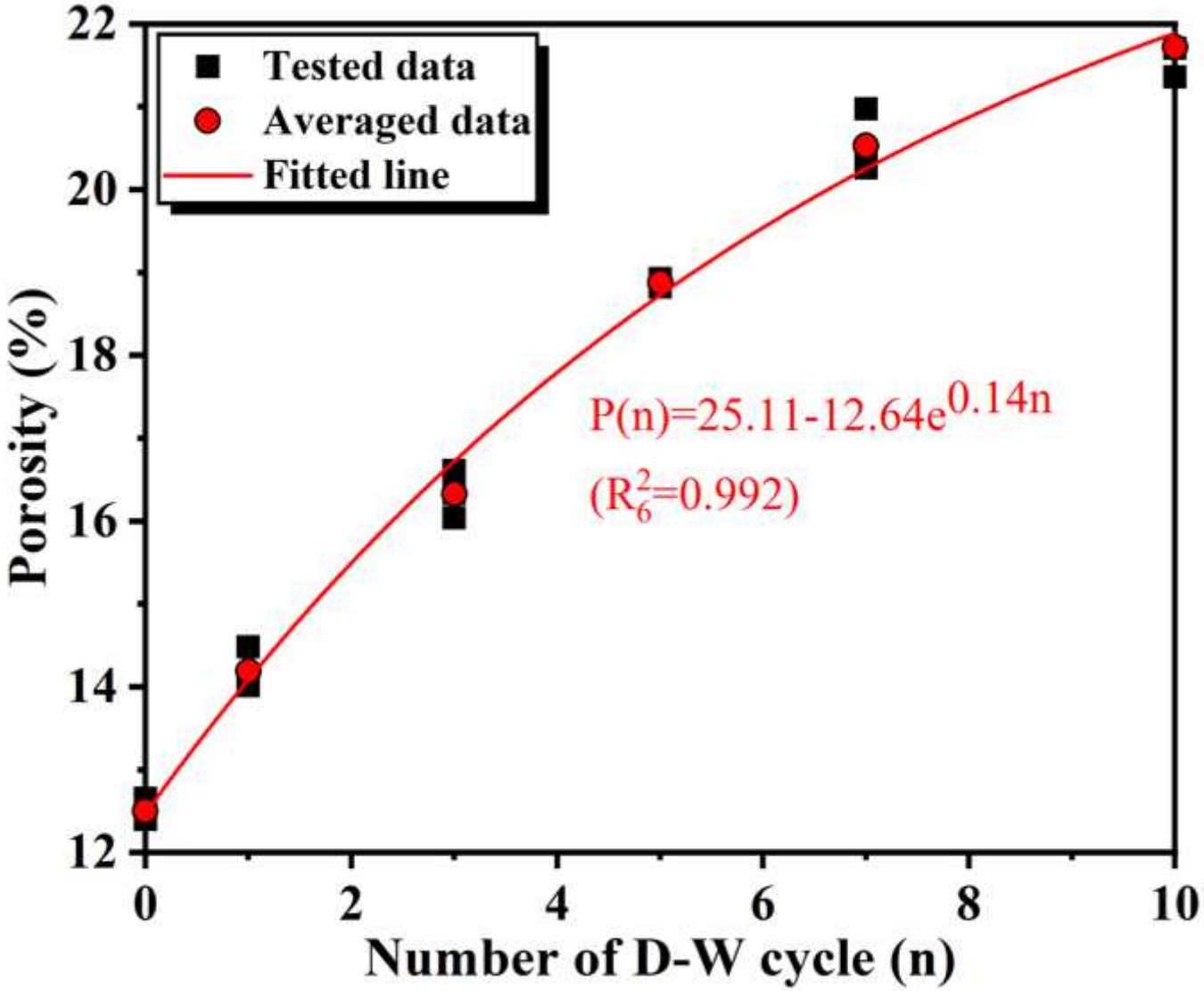

Figure 6

Porosity evolutions after different number of D-W cycles

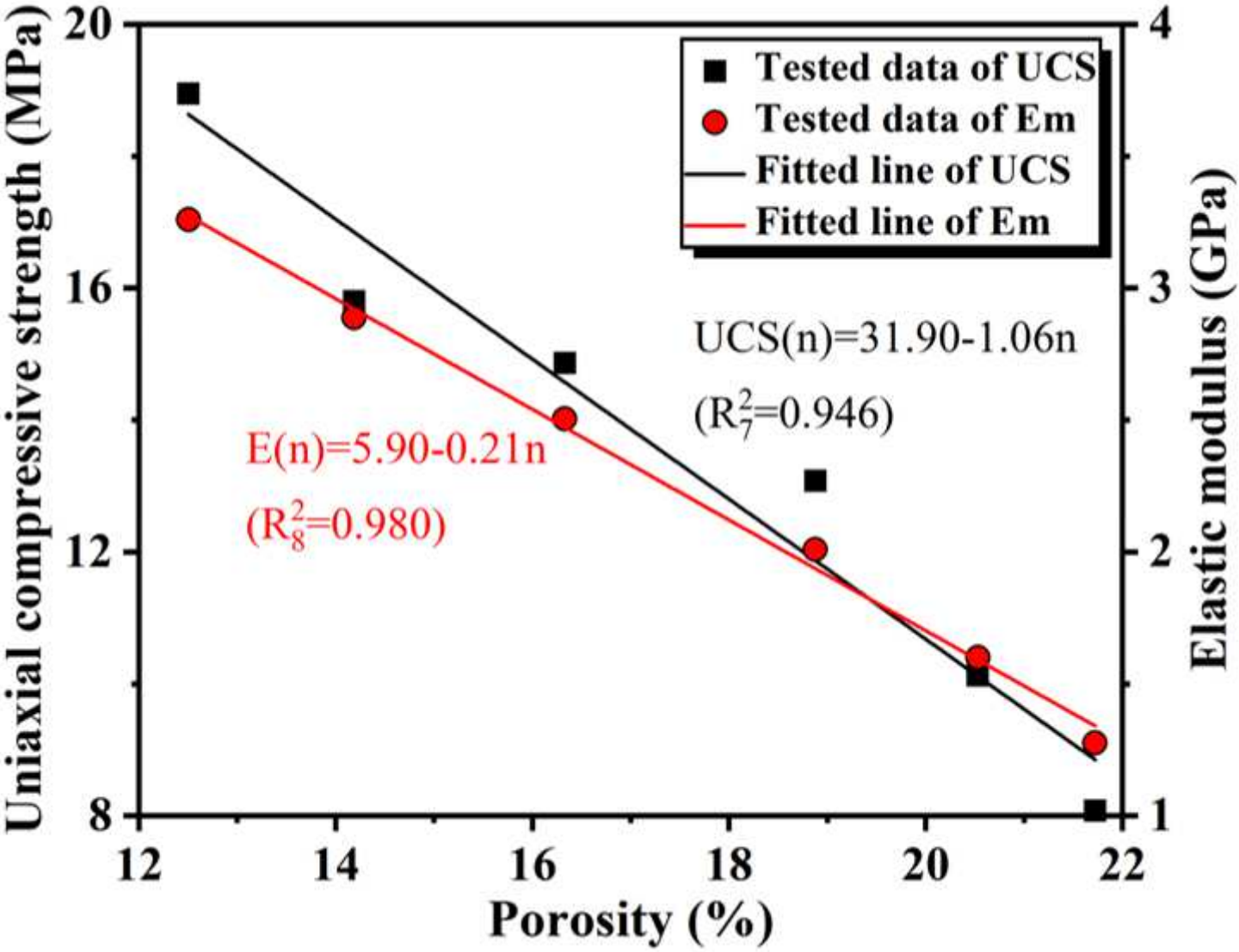

Figure 7

Evolutionary relationship between the uniaxial compressive strength, elastic modulus and porosity

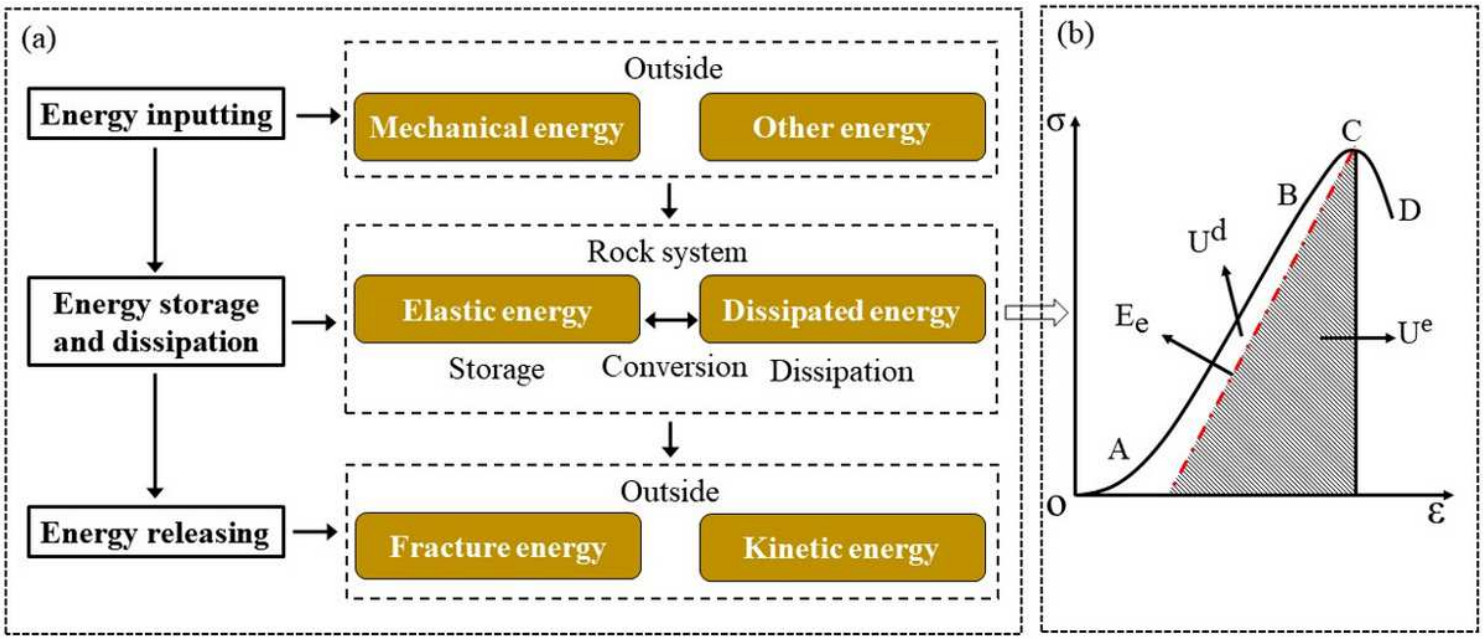

Figure 8

Forms of the energy of rock under uniaxial loading

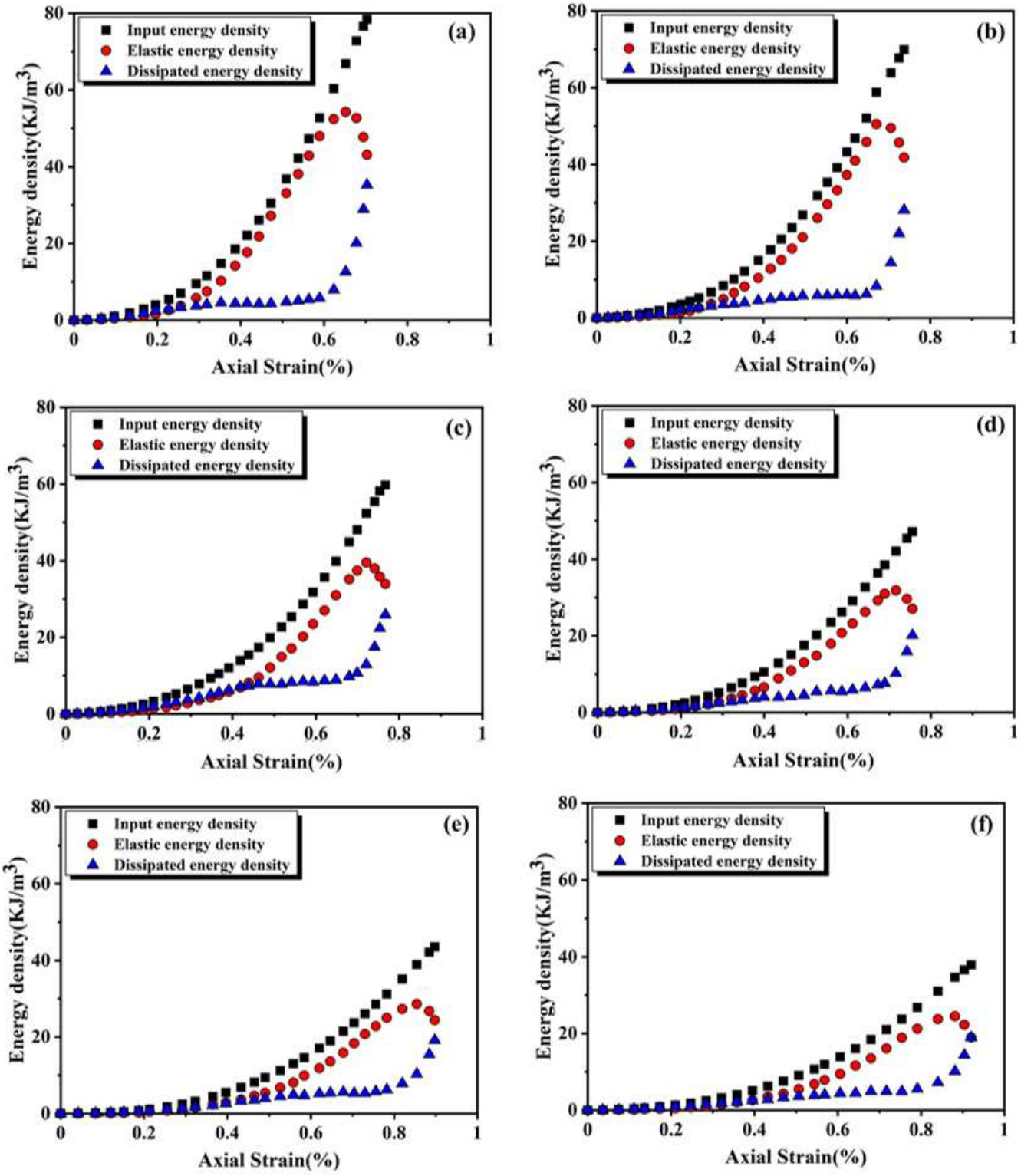

Figure 9

Energy evolution characteristic of the tested specimens subjected to: (a) Initial; (b) 1 cycles; (c) 3 cycles; (d) 5 cycles; (e) 7 cycles; (f) 10 cycles of D-W

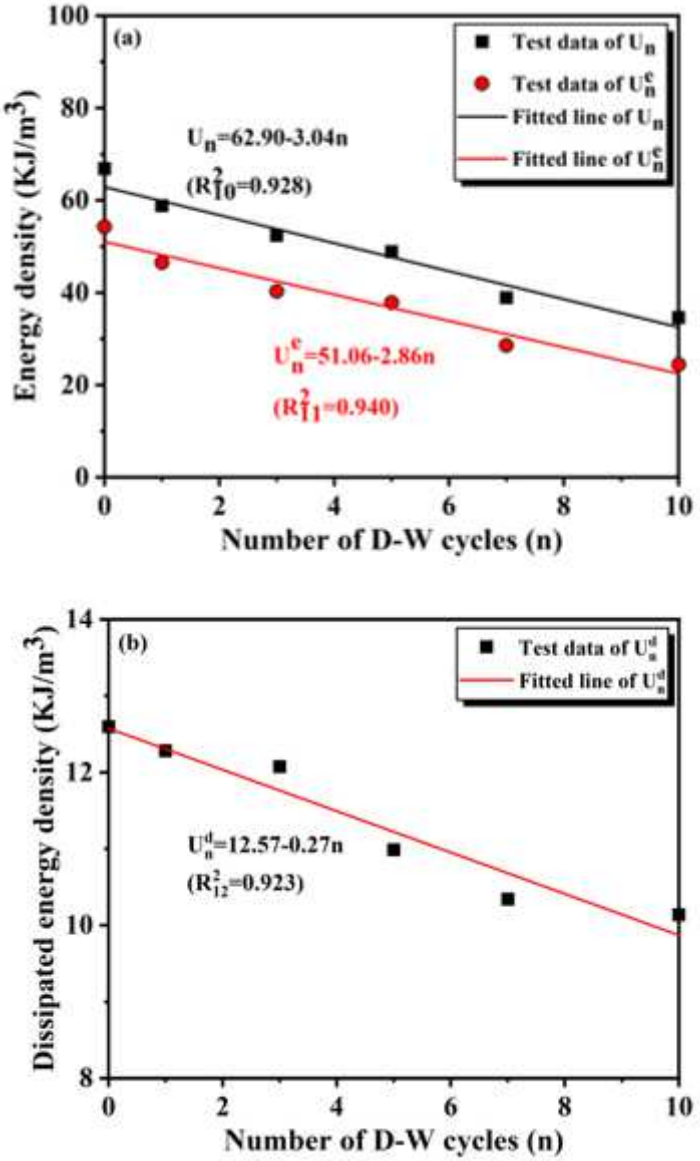

Figure 10

Please see the Manuscript PDF file for the complete figure caption.

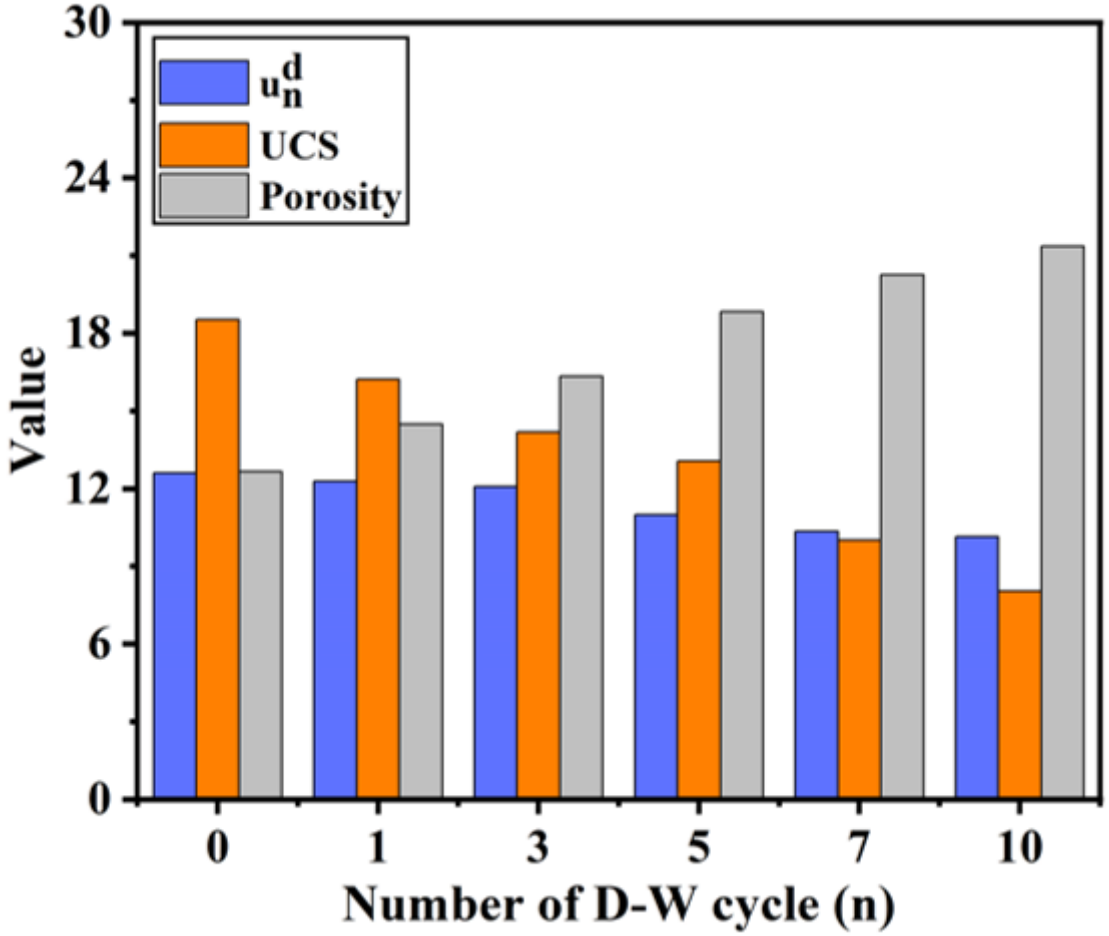

Figure 11

Please see the Manuscript PDF file for the complete figure caption.

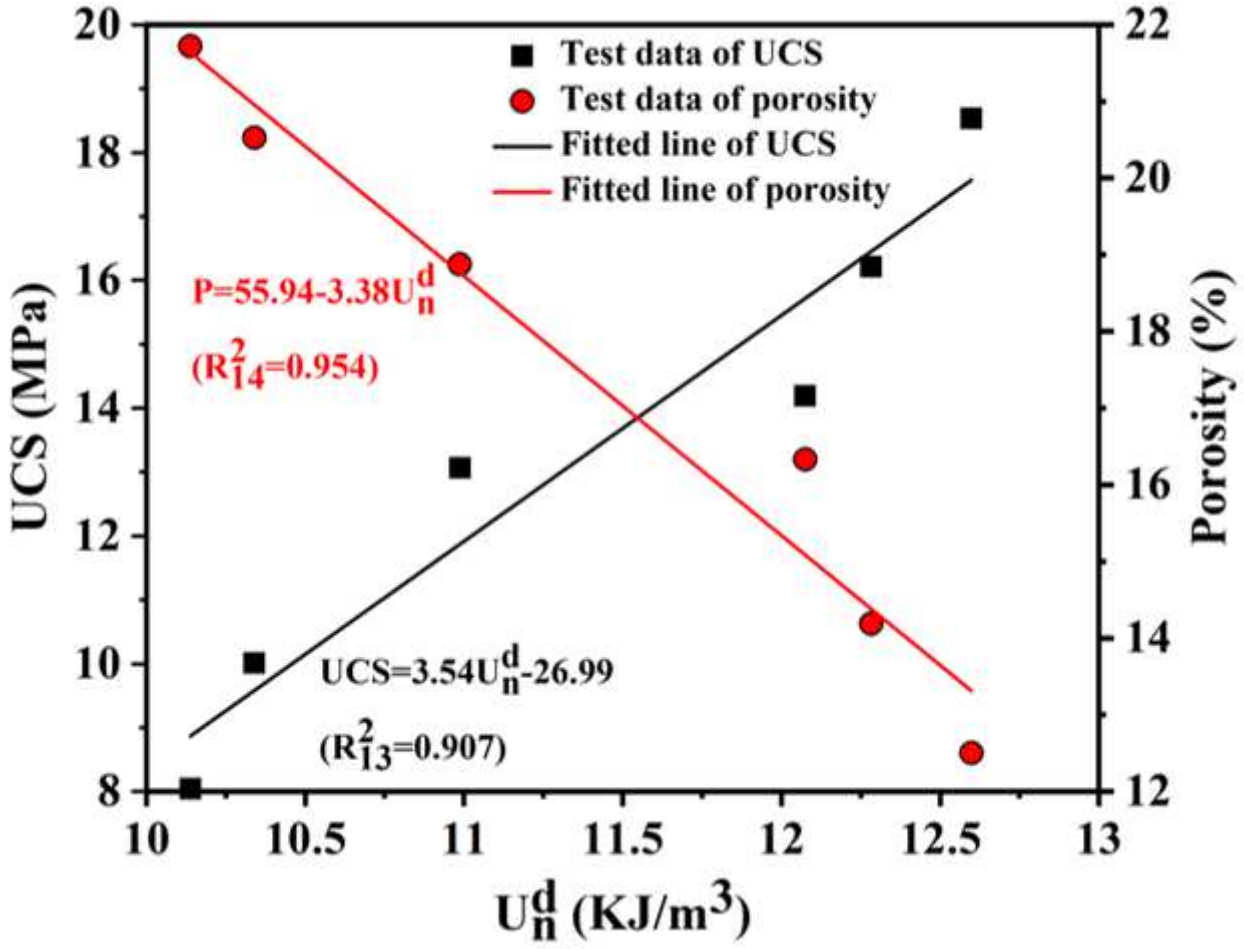

Figure 12

Relationship between dissipated energy and UCS and porosity

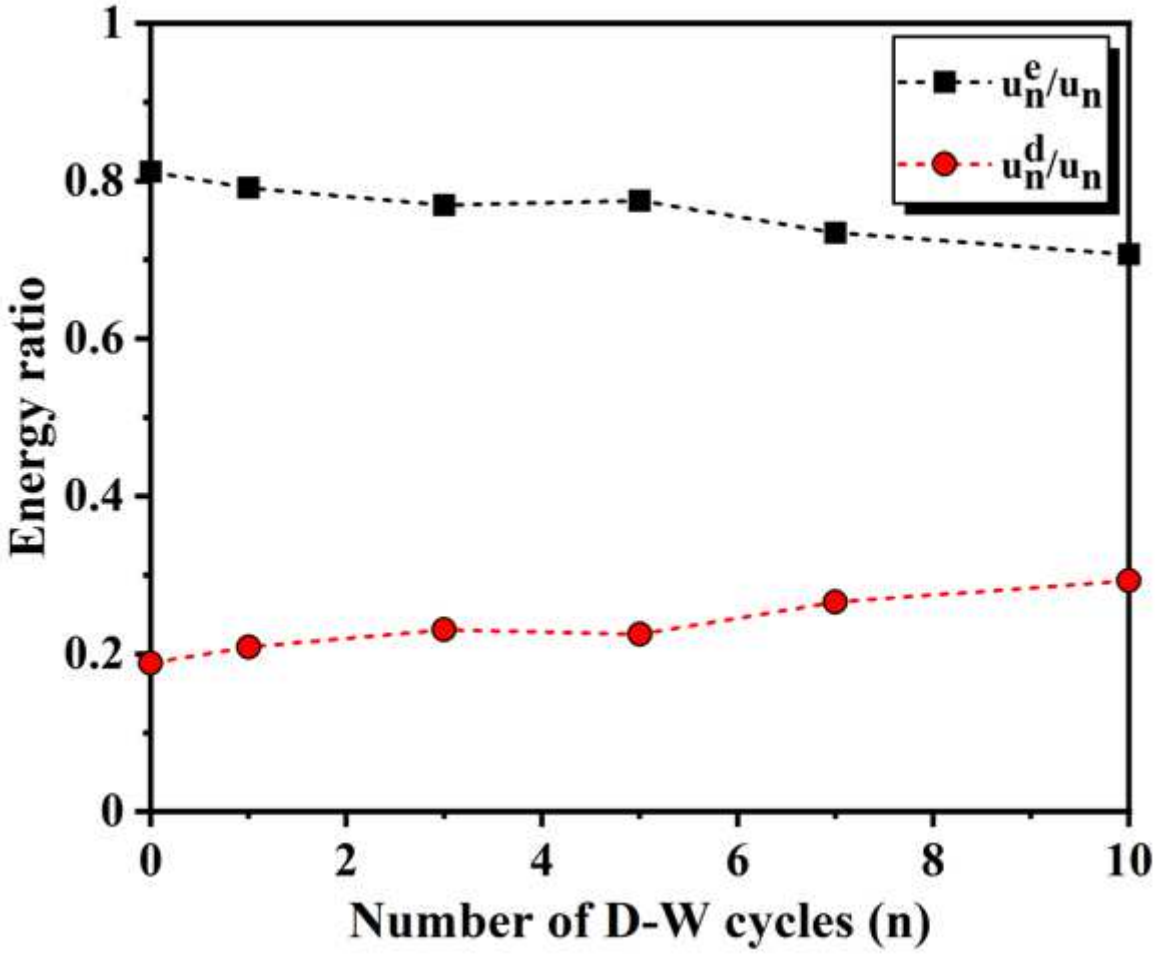

Figure 13

Relationship between the dissipation energy ratio and the number of D-W cycles